ChemComm

Oxygen-Atom Transfer Photochemistry of a Molecular Copper Bromate Complex

Journal:	*ChemComm*
Manuscript ID	CC-COM-08-2022-004403.R2
Article Type:	Communication

COMMUNICATION

Oxygen-Atom Transfer Photochemistry of a Molecular Copper Bromate Complex

Received 00th January 20xx,
Accepted 00th January 20xx

DOI: 10.1039/x0xx00000x

Gerard P. Van Trieste III,[a] Joseph H. Reibenspies,[a] Yu-Sheng Chen,[b] Debabrata Sengupta,[a] Richard R. Thompson,[a] and David C. Powers[a,*]

We report the synthesis and oxygen-atom transfer (OAT) photochemistry of $[Cu(tpa)BrO_3]ClO_4$. *In situ* spectroscopy and *in crystallo* experiments indicate OAT proceeds from a Cu–O fragment generated by sequential Cu–O bond cleavage and OAT from BrO_x to $[Cu(tpa)]^+$. These results highlight synthetic opportunities in M–O photochemistry and demonstrate the utility of *in crystallo* experiments to evaluating photochemical reaction mechanisms.

Reactive ligand-supported metal-oxygen (M–O) species are at the heart of oxygen-atom transfer catalysis in synthesis and biology and have featured prominently in the development of modern theories of metal-ligand (M–L) bonding. As a result, the synthesis and characterization of reactive metal–fragments have garnered significant interest. In the context of Cu oxygen chemistry, which are responsible for methane hydroxylation in both particulate monooxygenases (pMMOs)[1-5] and copper-doped porous materials, enormous synthetic effort has been directed towards the synthesis molecule mimics of catalyst structure and function.[6-11] These studies have resulted in the isolation of copper hydroxides, peroxides, hydroperoxides, and superoxide species, but the reactivity of terminal Cu–O species has thus far precluded isolation of this structural motif.[2]

Synthetic photochemistry can provide the opportunity to generate reactive species under cryogenic conditions and thus can enable observation and characterization of species that are short-lived under ambient conditions. To this end, photolysis of metal oxyanion complexes has been explored as a potential source of reactive metal oxygen fragments. In 2015, Zhang and coworkers reported that photolysis of Fe(III) bromate complexes afforded either Fe(IV) or Fe(V) oxo complexes depending on the structure of the supporting porphyrin ligand (Figure 1a).[12] In related studies of matrix isolated Fe(III) oxyanions complexes, Suslick and coworkers demonstrated that

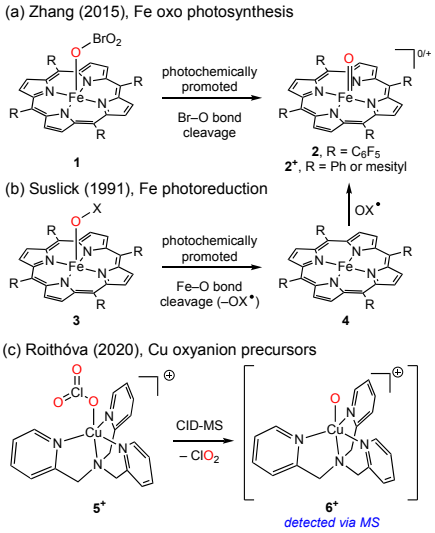

Figure 1. (a) Zhang and co-workers described ligand-dependent Fe oxo photochemistry of Fe(III) porphyrin bromate complexes. (b) Suslick and co-workers demonstrated that Fe–O homolysis is the initial step in the photochemical activation of a variety of oxyanion complexes and suggested subsequent OAT to the reduce metal fragment could generate M–O species. (c) Roithóva and co-workers utilized collision-induced disassociation mass spectrometry (CID-MS) to observe Cu–O fragment [**6**]$^+$.

oxyanion photochemistry was initiated by Fe–O bond homolysis and suggested that subsequent OAT from the extruded radical to the reduced metal center was responsible for oxo complexes observed in steady-state, solution-phase experiments (Figure 1b).[13-15] In the context of Cu oxyanion chemistry, in 2020 Roithová *et al.* reported the observation of Cu(tpa)O during collision-induced dissociation mass spectrometry (CID-MS) analysis of $[Cu(tpa)OClO_2]^+$ (Figure 1c).[16] While this experiment enabled observation of a transient Cu–O species, no spectroscopic or structural data were available.

Here we describe the synthesis, characterization, and OAT photochemistry of molecular copper bromate complex $[Cu(tpa)BrO_3]ClO_4$ ([**8**]ClO_4). Steady-state photolysis of [**8**]ClO_4 results in OAT to carbon monoxide as well as olefinic, benzylic, and aliphatic substrates. A combination of mass spectrometry, *in situ* spectroscopy, and *in crystallo* photochemical

[a] *Department of Chemistry, Texas A&M University, College Station, Texas 77843, United States.*
[b] *ChemMatCARS, University of Chicago, Argonne, IL 60439, United States.*
Electronic Supplementary Information (ESI) available: experimental procedures, spectral data, crystallographic data. See DOI: 10.1039/x0xx00000x

experiments are consistent with initial Cu–O bond cleavage to generate $[Cu(tpa)]^+$ and BrO_3. Subsequent OAT from $BrO_3^\bullet$ (or $BrO^\bullet$ obtained by decomposition of $BrO_3^\bullet$ to $BrO^\bullet$ and O_2) to Cu generates a transient Cu–O fragment that is responsible for substrate functionalization. These results provide new entry into reactive Cu–O species and highlight the power of *in crystallo* photochemistry to probe the reactions of molecular inorganic species.

Treatment of [Cu(tpa)Br]ClO_4 ([**7**]ClO_4) with $AgBrO_3$ affords [Cu(tpa)BrO_3]ClO_4 ([**8**]ClO_4) in 65% yield (Figure 2). The ^{1}H NMR spectrum of [**8**]ClO_4 features two paramagnetically shifted peaks at 10 and 29 ppm (Figure S1). The UV-vis spectrum of [**8**]ClO_4 in acetone displays a weak absorbance centered at 426 (ε = 2.3 × 10 $M^{-1}cm^{-1}$) and stronger absorbances at 710 (ε = 3.0 × 10^2 $M^{-1}cm^{-1}$), and 920 nm (ε = 5.4 × 10^2 $M^{-1}cm^{-1}$) (Figure S2). The IR spectrum of [**8**]ClO_4 displays spectral features at 831, 842, and 852 cm^{-1}, which are attributed to stretching modes of a Cu-bound bromate ligand (Figure S3).[17] Electrospray ionization mass spectrometry (ESI-MS) analysis of [**8**]ClO_4 displays a signal at *m/z* = 479.98 with the isotope distribution expected for **8**$^+$. Consistent with the *S* = 1/2 ground state typical of Cu(II) complexes, the X-band EPR spectrum of [**8**]ClO_4 measured at 4 K features an isotropic signal at *g* = 2.126 (Figure S4; for X-band EPR spectrum of [**7**]ClO_4, see Figure S5).

X-ray quality crystals were obtained by slow diffusion of diethyl ether into an acetone solution of [**8**]ClO_4; the solid-state

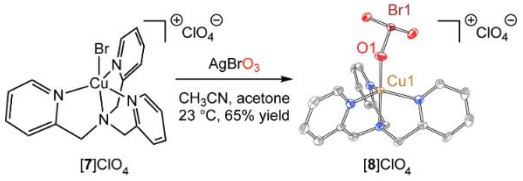

Figure 2. Treatment of Cu bromide [**7**]ClO_4 with $AgBrO_3$ affords Cu bromate [**8**]ClO_4. Displacement ellipsoid plot of [**8**]ClO_4. H-atoms and counter anions have been omitted for clarity. Ellipsoids drawn at 50% probability. Selected bond lengths (Å): Cu–O = 1.951(3), Cu–$N_{pyridine}$ = 2.072(4), and Cu–N_{amine} = 2.023(3).

structure is illustrated in Figure 2 (see Figure S6 and Table S1 for refinement details). The Cu(II) ion in [**8**]ClO_4 is five-coordinate and exhibits a distorted trigonal bipyramidal geometry (τ_5 = 0.77),[18] with the three pyridine donors from the tpa ligand occupying the equatorial plane. The apical sites are coordinated by the tertiary amine donor of the tpa ligand and an *O*-bound bromate ligand. The Cu–N distances in [**8**]ClO_4 (Cu–$N_{pyridine}$ = 2.072(4) Å, Cu–N_{amine} = 2.023(3) Å) are similar to other crystallographically characterized Cu(II)(tpa) complexes and the Cu–O distance (1.951(3) Å) is well-matched to crystallographically characterized Cu(II)(tpa) oxyanion complexes (Table S2).

Copper(II) bromate [**8**]ClO_4 participates in photochemically promoted oxygen-atom transfer (OAT) and hydrogen-atom abstraction (HAA) reactions, which are characteristic of the reactivity patterns of reactive M–O species (Figure 3). Photolysis (λ > 335 nm) of a CO-saturated CH_3CN solution of complex [**8**]ClO_4 afforded CO_2 (detected by GC analysis of the reaction headspace, Figure S7), which is the product of OAT to CO_2. Similar OAT to olefinic substrates was observed: Photolysis of [**8**]ClO_4 in the presence of styrene or 1-octene afforded epoxides **9** and **10** in 91% and 36% yields, respectively (Figures S8 and S9). Photolysis in the presence of 1,4-cyclohexadiene (bond dissociation energy (BDE) = 76.0 kcal mol^{-1})[19] yielded benzene (84% yield), the product of HAA (Figure S10). Photolysis of [**8**]ClO_4 in toluene (BDE = 89.7 kcal mol^{-1})[20] afforded benzyl alcohol in 76% yield (Figure S11)[21] and photolysis in the presence of cyclohexane (BDE = 99.5 kcal mol^{-1})[22] afforded a mixture of cyclohexanone (23% yield), cyclohexanol (17% yield), and bromocyclohexane (18% yield) (Figure S12). Photolysis of a CH_3CN solution of [**8**]ClO_4 in the presence of 1:1 H_8-toluene/ D_8-toluene provided a kinetic isotope effect (KIE; k_H/k_D) of 3.4(2) for benzylic hydroxylation, which is consistent with significant C–H cleavage in the rate-determining transition state (Figure S13). Photolysis of [**8**]ClO_4 in the presence of pentane (BDE = 97.5)[23] or benzene (BDE = 112.9)[20] resulted in no observed substrate oxidation. In no case were products of OAT or HAA observed without photolysis (*i.e.*, there are no background reactions with any of the substrates).

To gain additional insight into the mechanism of OAT and

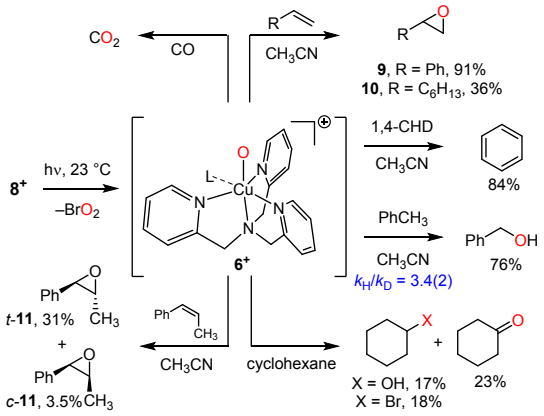

Figure 3. Summary of photochemically promoted substrate functionalization chemistry. Both oxygen-atom transfer (OAT) and hydrogen-atom abstraction reactivity have been observed and can be envisioned as arising from a transiently generated reactive CuO fragment (*i.e.*, $[Cu(tpa)(L)O]^+$ (**6**$^+$)); L = solvent or vacant coordination site.

the potential intermediacy of [CuO] species (*e.g.* **6**$^+$), we scrutinized the photochemical epoxidation of stereochemically defined 1,2-disubstituted olefins. Epoxidation of *cis*-β-methylstyrene is not stereospecific: Photolysis of [**8**]ClO_4 in the presence of *cis*-β-methylstyrene afforded a 10:1 mixture of *trans*:*cis*-**11** in 35% yield (Figure S14). For comparison, we also carried out the epoxidation of *cis*-β-methylstyrene with [Cu(tpa)]BF_4 ([**12**]BF_4) with PhIO and obtained a 10:1 mixture of *trans*:*cis*-**11** (Figure S15). The identical stereochemical outcome suggests that both photo-promoted and Cu(I) mediated processes proceed via a common intermediate, *e.g.* a CuO fragment. Taken with the primary KIE observed for benzylic hydroxylation of toluene, these data are consistent with stepwise substrate activation via carbon-centered radicals (*i.e.*, alkyl radicals generated by either radical addition to olefins or via H-atom abstraction (HAA) from alkanes).

In analogy to the oxyanion photochemistry described in Figure 1, we envisioned that the formation of a [CuO] intermediate could occur via direct photooxidation, *i.e.*, cleavage of the O–Br bond to generate $[Cu(tpa)O]^+$ (**6**$^+$) and

BrO_2, or via a photoreduction / OAT sequence, *i.e.*, initial cleavage of the Cu–O bond to generate a $[Cu(tpa)]^+$ fragment (**12**$^+$) and $BrO_3^\bullet$ following by OAT from $BrO_3^\bullet$ (or BrO derived thereof) to **12**$^+$. A combination of MALDI-MS, *in situ* spectroscopy data, and *in crystallo* photochemistry suggest the latter mechanism is operative under steady-state photolysis of [**8**]ClO_4.

Mass spectrometry data provides evidence for the ions expected from sequential photoreduction and subsequent OAT from $BrO_3^\bullet$ to **12**$^+$: $[Cu(tpa)]^+$ is the base ion in the MALDI-MS of [**8**]ClO_4 (indicated by the set of peaks at 353.0 and 355.0 *m/z* that are well matched to the simulated isotopic distribution) and $BrO_3^\bullet$ is detected as BrO_3^- via negative-mode MALDI-MS at 126.9 and 128.9 *m/z* (Figure 4a inset). OAT from extruded $BrO_3^\bullet$ to $[Cu(tpa)]^+$ would be accompanied by the evolution of BrO_2; negative-mode MALDI-MS features at 110.9 and 112.9 *m/z* correspond to expected isotopic distribution for BrO_2. Finally, CID-MS data indicates the formation of Cu–O fragment **6**$^+$ (Figure 4). In addition to mass spectrometry, the formation of BrO_2 is also evidence by *in situ* infrared (IR) spectroscopy: The IR spectrum of Cu bromate [**8**]ClO_4 in a KBr pellet displays characteristic bromate stretches at 831, 842, and 852 cm^{-1}. Photolysis of this KBr pellet results in the disappearance of those spectral features and the evolution of a new peak at 795 cm^{-1}, which is well-matched to a reported stretch for BrO_2 (Figure 4b).[23] The other stretching mode expected BrO_2 (*i.e.*, 845 cm^{-1}) overlaps with a stretching mode of the $[Cu(tpa)]^+$ fragment. Diffuse reflectance and X-band EPR spectra obtained after solid-state photolysis are depicted in Figures S16 and S17.

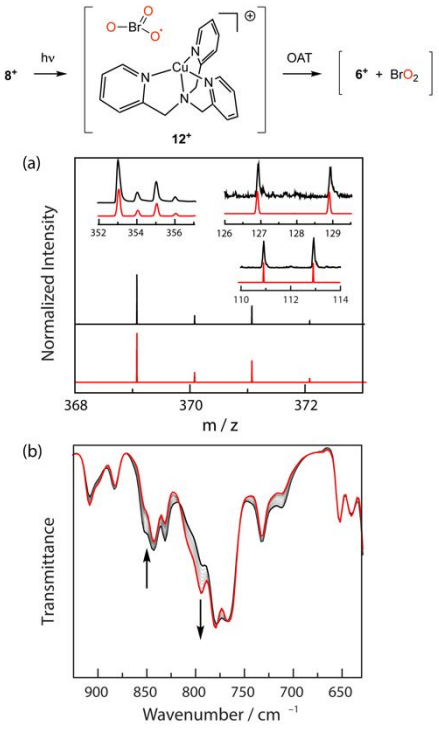

Figure 4. Photoreduction of **8**$^+$ by Cu–$OBrO_2$ homolysis followed by OAT from $BrO_3^\bullet$ to **12**$^+$ would generate **6**$^+$ and BrO_2. (a) CID-MS analysis shows peaks at 369.1 and 371.1 *m/z* which correspond to [**6**]$^+$; MALDI-MS analysis shows peaks at 110.9 and 112.9 *m/z* which correspond to BrO_2 (—), simulation (—) (inset); peaks at 126.9 and 128.9 *m/z* which correspond to photoextruded BrO_3 (—), simulation (—) (inset); and peaks at 353.0 and 355.0 *m/z* which correspond to $[Cu(tpa)]^+$ (—), simulation (—) (inset). (b) IR spectra collected during the photolysis of a KBr pellet of [**8**]ClO_4 shows a new peak at 795 cm^{-1}, which is attributed to BrO_2.

Attempts to characterize the photochemistry of [**8**]ClO_4 by low-temperature solution-phase spectroscopy have been stymied by a combination of insolubility in, or reaction with, common glassy solvents. To avoid these challenges and to build on emerging *in crystallo* photochemical strategies to characterize reactive species relevant to C–H functionalization, we were attracted to the potential to apply *in crystallo* photochemistry to directly visualize the primary photochemical events relevant to the OAT chemistry described above. We reasoned that photooxidation via BrO_2 loss would be differentiable from initial photoreduction via $BrO_3^\bullet$ elimination. To these ends, X-ray diffraction data was collected during 365 nm irradiation of a single crystal of [**8**]ClO_4 at 100 K using 30 keV synchrotron radiation. Solid-state reaction progress was monitored by free refinement of the Cu–$OBrO_2$ fragment.

Refinement of the X-ray diffraction data obtained following *in crystallo* photolysis of [**8**]ClO_4 are consistent with initial activation of the Cu–O bond (Figure 5, refinement details collected in Table S3). The most significant structural changes induced by photolysis are Cu–O elongation from 1.951(3) Å to 2.22(1) Å and Br–O contraction from 1.657(4) Å (avg.) to 1.53(1) Å (avg.). Accompanying Cu–O elongation, the Cu1–O1–Br1 angle opens from 124.28(2)° to 118.9(5)°. The average O–Br–O angles change minimally from 105.4(2)° to 103.6(8)°. In contrast to the significant elongation of the Cu–O vector, the Cu–N bonds are not significantly different following photolysis (Figure 5a). Based on comparison to the metrics of Cu(tpa)Cl,[24] *in crystallo* photoreduction of [**8**]ClO_4 to generate $BrO_3^\bullet$ and Cu(I) would be anticipated to elongate the Cu–N(4) vector significantly (0.4 Å in $[Cu(tpa)Cl]^+$). Furthermore, the optimized geometry of $[Cu(tpa)]^+$, featuring no fifth ligand as would be expected for *in crystallo* photoreduction, features a Cu–N(4) bond length of 2.2 Å (Table S4). As such, the metrics expected for Cu(I) are inconsistent with those observed following *in crystallo* photolysis. Instead, the observed structural parameters are more consistent with assignment of the *in crystallo* product of $Cu(II)^{2+}$ and BrO_3^-, which could arise from Cu–O homolysis followed by electron transfer (ET) from the initially formed Cu(I) to generate Cu(II). Rapid *in crystallo* ET may be driven by the dense crystal packing of [**8**]ClO_4: Unlike previous *in crystallo* photoreactions in which gaseous, closed-shell small molecule leaving groups (*e.g.* N_2 and CO) are extruded from the molecular photoprecursors,[25-29] *in crystallo*

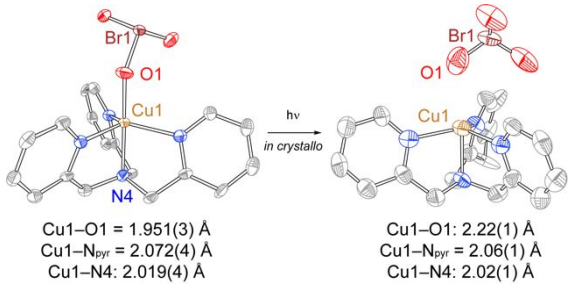

Figure 5. Displacement ellipsoid plots generated by *in crystallo* photochemistry of [**8**]ClO_4. Ellipsoids of [**8**]ClO_4 are drawn at 50% probability; following photolysis ellipsoids are drawn at 30% probability. H atoms and counter anions are removed for clarity.

Cu–O cleavage would generate a solid, reactive leaving group ($BrO_3^•$) that is held in proximity to the Cu(I) by virtue of crystal packing (Figure S18).

Finally, we examined the potential that $BrO_3^•$, produced by photochemical Cu–O homolysis, was the active oxidant in substrate functionalization chemistry (i.e. reactions pictured in Figure 3), we evaluated the photochemistry of a mixture of $KBrO_3$ and $(NH_4)_2S_2O_8$ in the presence of toluene. Photolysis of a mixture of $KBrO_3$ and $(NH_4)_2S_2O_8$ has previously been reported to afford $BrO_3^•$, which was detected by TA spectroscopy.[30] In our experiment, we irradiated a mixture of $KBrO_3$ and $(NH_4)_2S_2O_8$ in acetonitrile with 10 equivalents of toluene added. This reaction afforded a mixture of benzyl alcohol, benzaldehyde, benzoate (Figure S19), which contrasts the selective generation of benzyl alcohol during the photolysis of [**8**]ClO_4. $BrO_3^•$ is known[30] to undergo rapid decomposition to BrO and O_2 and the control experiment described here does not differentiate between whether OAT to $[Cu(tpa)]^+$ is accomplished by $BrO_3^•$ or reactive oxidants derived thereof. To verify that the observed reactivity is $BrO_3^•$ based, and not derived from transient intermediates of $(NH_4)_2S_2O_8$ photochemistry, we photolyzed a toluene solution of $(NH_4)_2S_2O_8$ and observed no oxidation products. Similar control experiments with cyclohexane are described in Figure S20.

In summary, we report the synthesis and OAT photochemistry of a molecular Cu bromate complex. Photoactivation results in net OAT to CO, olefinic substrates, and C–H bonds to afford CO_2, epoxides, and alcoholic products. *In crystallo* photochemistry is consistent with initial Cu–O bond cleavage and complementary mass spectrometry and *in situ* spectroscopy experimental suggest that initial Cu–O homolysis (*i.e.*, photoreduction) precedes the formation of a reactive Cu–O species that is responsible for substrate functionalization. These studies add to a growing body of literature on the prevalence of one-electron photochemistry of metal oxyanion complexes[31] and demonstrate new tools to elucidate the atomistic details of molecular photoreactions.

Author Contributions

G. P. V. T., D. S., and D. C. P. conceived of the project. G. P. V. T. and D. S. carried out experimental work. All authors participated in data analysis, manuscript writing, and editing.

Conflicts of interest

There are no conflicts to declare.

Acknowledgements

The authors acknowledge the U.S. Department of Energy (DOE), Office of Science, Office of Basic Energy Sciences, Catalysis Program (DE-SC0018977) and the Welch Foundation (A-1907). Structure determinations were collected at NSF's ChemMatCARS Sector 15, which is supported by NSF/CHE-1834750. Use of the Advanced Photon Source was supported by the U.S. DOE under Contract DE-AC02-06CH11357.

Notes and references

1 M. O. Ross, F. MacMillan, J. Wang, A. Nisthal, T. J. Lawton, B. D. Olafson, S. L. Mayo, A. C. Rosenzweig and B. M. Hoffman, *Science*, 2019, **364**, 566.
2 R. Davydov, A. E. Herzog, R. J. Jodts, K. D. Karlin and B. M. Hoffman, *J. Am. Chem. Soc.*, 2022, **144**, 377.
3 G. E. Cutsail, M. O. Ross, A. C. Rosenzweig and S. DeBeer, *Chem. Sci.*, 2021, **12**, 6194.
4 W. Peng, X. Qu, S. Shaik and B. Wang, *Nat. Catal.*, 2021, **4**, 266.
5 R. J. Jodts, M. O. Ross, C. W. Koo, P. E. Doan, A. C. Rosenzweig and B. M. Hoffman, *J. Am. Chem. Soc.*, 2021, **143**, 15358.
6 C. E. Elwell, N. L. Gagnon, B. D. Neisen, D. Dhar, A. D. Spaeth, G. M. Yee and W. B. Tolman, *Chem. Rev.*, 2017, **117**, 2059.
7 Y. Shimoyama and T. Kojima, *Inorg. Chem.*, 2019, **58**, 9517.
8 M. Srnec, R. Navrátil, E. Andris, J. Jašík and J. Roithová, *Angew. Chem. Int. Ed.*, 2018, **57**, 17053.
9 D. Maiti, H. R. Lucas, A. A. Narducci Sarjeant and K. D. Karlin, *J. Am. Chem. Soc.*, 2007, **129**, 6998.
10 D. Maiti, D.-H. Lee, K. Gaoutchenova, C. Wuertele, M. C. Holthausen, A. A. Narducci Sarjeant, J. Sundermeyer, S. Schindler and K. D. Karlin, *Angew. Chem., Int. Ed.*, 2008, **47**, 82.
11 S. Hong, S. M. Huber, L. Gagliardi, C. C. Cramer and W. B. Tolman, *J. Am. Chem. Soc.*, 2007, **129**, 14190.
12 T.-H. Chen, N. Asiri, K. W. Kwong, J. Malone and R. Zhang, *Chem. Commun.*, 2015, **51**, 9949.
13 D. N. Hendrickson, M. G. Kinnaird and K. S. Suslick, *J. Am. Chem. Soc.*, 1987, **109**, 1243.
14 K. S. Suslick, J. F. Bautista and R. A. Watson, *J. Am. Chem. Soc.*, 1991, **113**, 6111.
15 K. S. Suslick and R. A. Watson, *Inorg. Chem.*, 1991, **30**, 912.
16 N. R. M. de Kler and J. Roithova, *Chem. Commun.*, 2020, **56**, 12721.
17 A. V. Levanov, I. B. Maksimov, O. Y. Isaikina, E. E. Antipenko and V. V. Lunin, *Rus. J. Phys. Chem. A*, 2016, **90**, 1312.
18 A. W. Addison, T. N. Rao, J. Reedijk, J. van Rijn and G. C. Verschoor, *J. Chem. Soc. Dalton Trans.*, 1984, 1349.
19 Y.-R. Luo, *Handbook of Bond Dissociation Energies in Organic Compounds*, CRC Press, Boca Raton, 2002.
20 S. J. Blanksby and G. B. Ellison, *Acc. Chem. Res.*, 2003, **36**, 255.
21 Benzyl alcohol is obtained from the analogous photolysis of [**8**]BF_4, thus perchlorate is not the oxygen source for substrate functionalization.
22 L. Bu, P. N. Ciesielski, D. J. Robichaud, S. Kim, R. L. McCormick, T. D. Foust and M. R. Nimlos, *J. Phys. Chem. A*, 2017, **121**, 5475.
23 J. Koelm, A. Engdahl, O. Schrems and B. Nelander, *Chem. Phys.*, 1997, **214**, 313.
24 W. T. Eckenhoff and T. Pintauer, *Inorg. Chem.*, 2007, **46**, 5844.
25 A. Das, J. H. Reibenspies, Y.-S. Chen and D. C. Powers, *J. Am. Chem. Soc.*, 2017, **139**, 2912.
26 A. Das, Y.-S. Chen, J. H. Reibenspies and D. C. Powers, *J. Am. Chem. Soc.*, 2019, **141**, 16232.
27 A. Das, C.-H. Wang, G. P. Van Trieste, C.-J. Sun, Y.-S. Chen, J. H. Reibenspies and D. C. Powers, *J. Am. Chem. Soc.*, 2020, **142**, 19862.
28 T. Schmidt-Räntsch, H. Verplancke, J. N. Lienert, S. Demeshko, M. Otte, G. P. Van Trieste III, K. A. Reid, J. H. Reibenspies, D. C. Powers, M. C. Holthausen and S. Schneider, *Angew. Chem. Int. Ed.*, 2022, **61**, e2021156.
29 A. Das, G. P. Van Trieste and D. C. Powers, *Comments Inorg. Chem.*, 2020, **40**, 116.
30 Z. Zuo and Y. Katsumura, *J. Chem. Soc., Farady Trans.*, 1998, **94**, 3577.
31 Y. Abderrazak, A. Bhattacharyya and O. Reiser, *Angew. Chem. Int. Ed.*, 2021, **60**, 21100.